Prepared for submission to JCAP

Searching for Exploding Black Holes

Xavier Boluna,[a,b] **Stefano Profumo,**[a,b] **Juliette Blé,**[b,c,d] **and Dana Hennings**[b,e,f]

[a]Department of Physics, University of California, Santa Cruz Santa Cruz, CA 95064, USA
[b]Santa Cruz Institute for Particle Physics, Santa Cruz, CA 95064, USA
[c]Université Paul Sabatier, 118 Route de Narbonne, F-31062 Toulouse, France
[d]Université Grenoble Alpes, 621 Avenue Centrale, F-38400 Saint Martin d'Hérès, France
[e]The Peddie School, 201 South Main Street Hightstown, NJ 08520, USA
[f]Wesleyan University, 45 Wyllys Ave, Middletown, CT 06459, USA

E-mail: profumo@ucsc.edu

Abstract. The observation of the final stages of the evaporation of a light black hole, which Hawking referred to as "black hole explosion", would offer critical insights on the existence of new degrees of freedom as well as on quantum gravity and high-energy physics phenomena. Here, we explore, review, and revisit the observational features and rates expected for nearby, light, evaporating black holes, and we reassess and compare sensitivity estimates for a broad range of observatories. We then focus on the search for candidate black hole explosions in archival data from the Fermi Large Area Telescope and Gamma-ray Burst Monitor, and outline possible future observational campaigns.

Contents

1 Introduction

While the identity of dark matter (DM) is still unknown, its role in shaping the universe as we observe it both at early and late times has now come into sharp definition [1]. In parallel, the quest for a consistent quantum theory of gravity is far from over (see e.g. [2] and references therein). Notably, at the intersection of these two major, open problems potentially lie black holes of non-stellar origin, or Primordial Black Holes (PBHs, see e.g. [3–5] for recent reviews of formation mechanism, constraints, and search strategies). The observation of the final stages of black hole evaporation would provide clues on the number of dark sector degrees of freedom independent of them being secluded from the visible sector [6–8], and would shed light on physics at energy scales close to the Planck scale, thus offering insights on quantum gravity (see e.g. [9] and references therein).

As envisioned by Hawking almost a half century ago [10, 11], simple physics relating the temperature and mass of black holes determines the runaway process of black hole "explosions" (to use the same expression Hawking introduced in Ref. [10]) and sets the universal luminosity of such events. In fact, both the luminosity and the *lightcurve* (photon emission as a function of time) of black hole evaporation are entirely fixed by the mass spectrum, charge, and spin of the degrees of freedom the hole can evaporate to, and by the photon yield associated with those same degrees of freedom. In the standard model, this luminosity and light curve are known with great precision, allowing for a sharp answer to the question of whether black hole explosions are detectable with current technology [3].

Should additional, secluded degrees of freedom exist beyond the Standard Model, they would impact the lightcurve and luminosity both by accelerating the evaporation rate by

allowing the hole to emit a broader set of particle species, and by, possibly, producing additional photons from the decay and fragmentation of the evaporation products (early work in this direction was presented in Ref. [6], and more recent and in-depth studies appeared more recently [7, 8]).

Broadly, a PBH explosion would resemble a short gamma-ray burst. However, key differences exist:

(i) the luminosity of an exploding PBH increases following a completely *universal* lightcurve, and *never decreases*, at least assuming the existence of no additional degrees of freedom to the SM;

(ii) the spectrum of the gamma-ray emission, under the same assumption, is also universal;

(iii) PBH explosions must be *local*, i.e. within, at most, a few parsecs of Earth, to be detectable by current and planned facilities [12]; the evaporation process thus potentially (albeit not necessarily) exhibits *proper motion*, depending on the age, distance, and PBH direction of motion relative the the line of sight;

(iv) finally, the intrinsic luminosity of exploding PBHs is exactly the same for every event.

The study we present here is not the first attempt at searching for PBH explosions with gamma-ray observations. The rate of explosions, on different time-scales and energy, has been constrained by direct observations with a number of different telescopes: in approximate order of appearance, limits have been obtained by the H.E.S.S. array of Cherenkov telescopes [13] (see also the recent update in Ref. [14]), MILAGRO [15], the Fermi Large Area Telescope (LAT) [16], the VERITAS Cherenkov telescope array [17] and the water Cherenkov detector HAWC [18] that, at present, produced the most stringent constraints on the local "explosion rate", at $\dot{n} < 3400$ pc^{-3} yr^{-1} at 99% C.L.. Cline and collaborators have scoured early GRB data sets for events that could be potentially associated with PBH explosions [19–23]. Ukawatta et al [24] considered the prospects for utilizing a *network* of widely separated non-imaging space-based detectors ("inter-planetary network", IPN) that could determine if a high-energy photon burst is at cosmological distances or whether it is nearby; intriguingly, several putative events, detected by three or more IPN spacecrafts have been associated with possibly nearby events [24].

The remainder of this paper is structured as follows: In the next section 2 we review the photon spectrum and lightcurve of exploding PBH (note that other channels of PBH evaporation can be in principle used for detection, including notably cosmic rays [25, 26], neutrinos [27], and gravitational waves [28, 29]); the following sec. 3 discusses theoretical expectations for the density and rate of PBH explosions compatible with all other observational constraints, and presents a very compact formula for the rate of explosions per unit volume per unit time today $\dot{n}_{\rm PBH}$ for a given generic *initial* PBH mass function ψ_i, in the form $\dot{n}_{\rm PBH} = \rho_{\rm DM}\psi_i(M_U)/(3t_U)$, where $M_U \simeq 5.1 \times 10^{14}$ grams is the mass corresponding to a lifetime equal to the age of the universe today, t_U. Sec. 4 discusses the sensitivity estimate for a PBH at a given distance and time to complete evaporation for a number of observatories, as well as the sensitivity to the presence of secluded degrees of freedom at a given mass-scale. Our results of searching for candidate PBH explosion in gamma-ray burst catalogues are presented in sec. 5, and our discussion, outlook, and conclusions in sec. 6.

2 Photon emission from exploding black holes

The instantaneous and integrated photon emission from black holes of a given mass, charge, and spin is by now well understood and readily available via publicly accessible numerical codes such as `BlackHawk` [30], that we utilize herein. The production of photons stems both from direct evaporation ("primary" photons) and from the indirect production of photons from radiation or decay of different evaporation products ("secondary" photons). A particle species i of mass m spin s, angular momentum quantum numbers (l, m), charge q is emitted by a black hole (BH) (which we take as having a mass M, charge Q and angular momentum Ω) with energy E at a rate[1]

$$\frac{\mathrm{d}^2 N_i}{\mathrm{d}E\ \mathrm{d}t}(E) = \frac{1}{2\pi}\frac{\Gamma_{E,s,q,l,m}(M,Q,\Omega,...)}{e^{E/T_{\rm BH}} - (-1)^{2s}}\theta(E-m), \tag{2.1}$$

where $T = \kappa/2\pi$ is the BH temperature (κ is the surface gravity of the BH, and $T = 1/(8\pi M)$, in natural units, for uncharged, non-spinning Shcwarzschild black holes), and Γ are the so called "greybody factors", that depend on both the particle and the BH quantum numbers, mass, and energy [31]. The flux of secondary particles j is computed from Eq. (2.1) as

$$\frac{\mathrm{d}^2 N_j}{\mathrm{d}E\ \mathrm{d}t}(E) = \int_0^\infty \sum_i \mathrm{BR}_{i\to j}(E,E')\frac{\mathrm{d}^2 N_i}{\mathrm{d}E'\ \mathrm{d}t}(E')\mathrm{d}E' \tag{2.2}$$

where $\mathrm{BR}_{i\to j}(E,E')$ is the particle physics branching ratio describing how a particle j of energy E is eventually produced from particle i of energy E'.

In the standard model, the approximate photon emission per unit time from a BH of temperature $T_{\rm BH}$, integrated over the energy range 0.3 GeV to 100 GeV, is, at late times, [31]

$$\dot{N}_\gamma \simeq 1.4\times 10^{29}\left(\frac{T_{\rm BH}}{\rm TeV}\right)^{1.6}\frac{1}{\rm sec}, \tag{2.3}$$

which translates into a photon flux, from the hole, at a distance d, of

$$\phi_\gamma \simeq 1.2\times 10^{-9}\left(\frac{\rm pc}{d}\right)^2\left(\frac{T_{\rm BH}}{\rm TeV}\right)^{1.6}\frac{1}{\rm sec\ cm^2}; \tag{2.4}$$

As a function of the hole's mass $M_{\rm BH}$, this, in turn, reads

$$\phi_\gamma \simeq 1.1\times 10^{-9}\left(\frac{\rm pc}{d}\right)^2\left(\frac{10^{10}\ \rm g}{M_{\rm BH}}\right)^{1.6}\frac{1}{\rm sec\ cm^2}. \tag{2.5}$$

For a non-spinning black hole, the mass evolution of the black hole with time can be inferred from the emission rates above and from the temperature-mass relation, and can be schematically cast in the form

$$\frac{dM}{dt} = -\frac{f(M)}{M^2,} \tag{2.6}$$

with the "Page coefficient" $f(M)$ dependent on the particles that the hole can evaporate to; as a result, and assuming that $f(M)\sim\alpha$ is constant at large-enough temperatures, the lifetime of a light PBH goes as $\tau \sim M^3/(3\alpha)$. In particular, $\tau(M_U) = t_U$ for $M_U \simeq 5.1\times 10^{14}$ g.

[1] Note that the particle energy may be corrected by the effective chemical potentials due to spin or charge coupling [3]

2.1 The effect of additional dark degrees of freedom

As described above, BH evaporation proceeds into any degree of freedom with mass close to, or below, the BH temperature. As such, independent of the interaction properties, any beyond-the-Standard-Model (BSM) "dark" degree of freedom contributes to the evaporation rate of BHs. Depending on whether the additional BSM degrees of freedom lead to the secondary production of photons upon their decay/hadronization, the BH lightcurve (photon emission rate as a function of the BH mass) is affected, and generically the BH lifetime reduced. This was noted in the literature long ago [6], and explored in some detail, including from the standpoint of direct detection of exploding BH, more recently in [7, 8]. Also note that for very large BSM sectors, the direct observation of BHs of (presumably) astrophysical origin puts constraints on the number of light degrees of freedom, as noted e.g. in [32].

Suppose that at a time t_D the evaporation rate $\alpha \to \alpha + \alpha_D$, because of the appearance of "dark" degrees of freedom; for simplicity, assume that such BSM degrees of freedom be in fact completely dark, thus not contributing to photon emission; also for simplicity, assume both α, α_D constant in the range of mass/time of interest; the evolution of mass with time reads:

$$M^3(t) = M_0^3 - 3\alpha t \ (t < t_D); \tag{2.7}$$

$$M^3_{t>t_D}(t) = M_0^3 - 3\alpha t_D - 3\alpha_D(t - t_D) = M(t)^3 - 3(\alpha_D - \alpha)(t - t_D). \tag{2.8}$$

As a result, with the additional degrees of freedom, the time t' at which $M_{t>t_D}(t) = M(t')$ is

$$t' = t + \frac{\Delta\alpha}{\alpha}(t - t_D), \quad \Delta\alpha = \alpha_D - \alpha > 0. \tag{2.9}$$

Thus, given the lightcurve $\phi_\gamma(t)$ for "standard" evaporation, with the additional degrees of freedom, at $t > t_D$

$$\phi_\gamma(t) \to \phi_\gamma\left(t + \frac{\Delta\alpha}{\alpha}(t - t_D)\right).$$

Defining τ the time to complete evaporation (happening at $t = t_\dagger$), i.e. $\tau = t_\dagger - t$, and $\tau_D = t_\dagger - t_D$, one has the following equivalent parameterization for the modified lightcurve:

$$\phi^D_\gamma(\tau) = \phi_\gamma(\tau), \ [\tau \geq \tau_D]; \tag{2.10}$$

$$\phi^D_\gamma(\tau) = \phi_\gamma\left(\tau - \frac{\Delta\alpha}{\alpha}\tau_D(\tau_D - \tau)\right), \ [\tau < \tau_D] \tag{2.11}$$

To match the time of complete evaporation, the equations above need to be shifted by $\tau \to \tau + \frac{\Delta\alpha}{\alpha}\tau_D$, leading to the final expression

$$\phi^D_\gamma(\tau) = \phi_\gamma\left(\tau + \frac{\Delta\alpha}{\alpha}\tau_D\right), \ [\tau \geq \tau_D]; \tag{2.12}$$

$$\phi^D_\gamma(\tau) = \phi_\gamma\left(\left(1 + \frac{\Delta\alpha}{\alpha}\right)\tau\right), \ [\tau < \tau_D] \tag{2.13}$$

Notice that, approximately, the relation between τ_D and M_D, the mass scale of the dark degrees of freedom (assumed to be mass degenerate), reads

$$M_D \simeq \frac{(3\alpha\tau_D)^{-1/3}}{8\pi}. \tag{2.14}$$

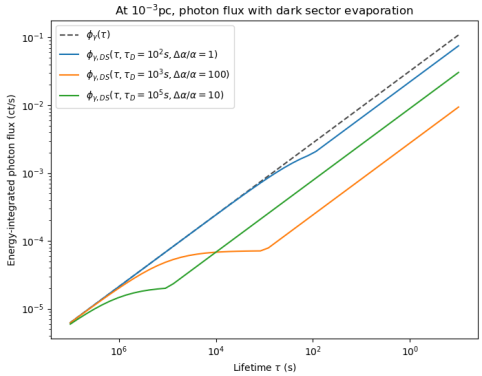

Figure 1. Lightcurves from BH evaporation with ($\phi_{\gamma,\mathrm{DS}}$) and without ($\phi_\gamma$) evaporation to dark sector degrees of freedom (where the dark sector is assumed to not produce any photons). $\Delta\alpha/\alpha$ defines the relative contribution of the dark degrees of freedom to the evaporation rate without them, whereas τ_D denotes the remaining lifetime of the hole.

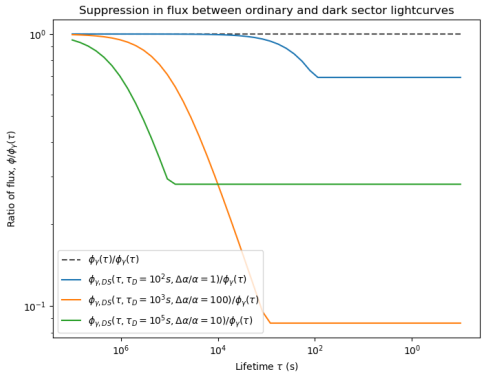

Figure 2. The ratio of the dark sector lightcurves to the ordinary lightcurve, for the same parameter choices as in Fig. 1.

Fig. 1 compares the ordinary lightcurve from BH evaporation, as a function of the remaining lifetime τ, with the lightcurve expected with both a relative increase (compared to the standard case) in the number of degrees of freedom $\Delta\alpha/\alpha = 1,\ 10,\ 100$, and with the times corresponding to the mass/energy scale of the new degrees of freedom (see Eq.(2.14) above), $\tau_D = 10^2,\ 10^3,\ 10^5$ sec. As expected, dark sector evaporation reduces the total number of photons emitted in the EBH lifetime. Using the same parameters, we show the ratio of fluxes – the dark sector lightcurve divided by the ordinary lightcurve – to visualize this deviation over time in Fig. 2. At late times, large values of $\Delta\alpha/\alpha$ can diminish the peak flux by orders of magnitude.

Measurements of the lightcurve, and, crucially, of the *derivative* thereof, would yield information both on the number of dark degrees of freedom $\Delta\alpha$, and of the associated energy/mass M_D and time scale relative to complete evaporation τ_D. One can compute the time corresponding to the ratio going from its early time asymptote of 1, to its late-time value $R_\dagger$ close to complete evaporation (the value the curves reach on the right of Fig. 2). In particular, the time at which the minimum of the ratio is reached is a direct proxy for τ_D, while the depth of the late-time ratio $R_\dagger = \phi_\gamma^D(\tau_D)/\phi_\gamma(\tau_D)$ correlates with $\Delta\alpha/\alpha$: assuming (as it is largely the case, especially at low energy) that $\phi_\gamma(\tau) \sim \tau^{-\beta}$, with $\beta \sim 1/3$, we have

$$R_\dagger = \frac{\phi_\gamma^D(\tau_D)}{\phi_\gamma(\tau_D)} \simeq \frac{\tau_D^{-\beta}\left(1+\frac{\Delta\alpha}{\alpha}\right)^{-\beta}}{\tau_D^{-\beta}} = \left(1+\frac{\Delta\alpha}{\alpha}\right)^{-\beta}, \tag{2.15}$$

allowing for a direct estimate of $\Delta\alpha$ from a measurement of $R_\dagger$. Notice that it can be readily shown that $\beta \simeq 1/3$ is a generic prediction in the limit $E_\gamma \ll T$: in that limit,

$$\phi_\gamma(E_\gamma \ll T) \sim \frac{1}{e^{E_\gamma/T}-1} \sim T$$

and since

$$M(\tau) \simeq \left(M_0^3 - 3\alpha\left(t_\dagger - \tau\right)\right)^{1/3} = \left(M_0^3 - 3\alpha\left(\frac{M_0^3}{\alpha} - \tau\right)\right)^{1/3} = (3\alpha\tau)^{1/3},$$

we get that $\phi_\gamma \sim T \sim 1/M(\tau) \sim \tau^{-1/3}$.

3 Density and explosion rates for evaporating black holes

Constraints on the relative contribution of PBHs to the dark matter mass density are usually cast in terms of the maximal fraction $f_{\rm max}(m)$ of the cold dark matter density that can consist of PBH of a given, single mass m. The (maximal possible) number density of such monochromatic PBHs at a mass $m_{\rm PBH}$ is then simply cast, in terms of the local dark matter density $\rho_{\rm DM}(\vec{r})$, as $n_{\rm PBH} = f_{\rm max}(m_{\rm PBH})\rho_{\rm DM}(\vec{r})/m_{\rm PBH}$. For non-monochromatic mass functions, say for a mass function $\psi(M) \propto M\frac{dn_{\rm PBH}}{dM}$ normalized as customary to $f_{\rm PBH}$, i.e.

$$\int dM\psi(M) = f_{\rm PBH}, \tag{3.1}$$

the equivalent constraints can be cast as [33]

$$\int dM \frac{\psi(M)}{f_{\rm max}(M)} < 1. \tag{3.2}$$

Usually, $\psi(M) = \psi_i(M)$ indicates the mass function at PBH creation. One then needs to time-evolve the mass function in the standard way [33], obtaining a final mass function ψ_f (see also [34])

$$\frac{\psi_f(M)}{M} = \frac{dn}{dM} = \frac{dn}{dM_i}\frac{dM_i}{dM}, \tag{3.3}$$

where

$$M_i^3 = M^3 + 3\tilde{\alpha}(M)t, \qquad \frac{dn}{dM_i} = \frac{\psi_i(M_i)}{M_i}. \tag{3.4}$$

Thus we find that

$$\frac{dn}{dM} = \psi_i\left(\left(M^3 + 3\tilde{\alpha}(M)t\right)^{1/3}\right)\frac{M^2}{M^3 + 3\tilde{\alpha}(M)t}, \tag{3.5}$$

assuming that $\tilde{\alpha}(M) \simeq$ const (precisely, that $|d\tilde{\alpha}(M)/dM|t \ll M^2$, which is abundantly true in the standard case). Thus, the rate of explosions today, i.e. the rate at which the mass function crosses $M = 0$ per unit volume per unit time corresponds to

$$\dot{n}_{\rm PBH} = \frac{dn}{dM}\left(-\frac{dM}{dt}\right) = \rho_{\rm DM}\psi_i\left(\left(M^3 + 3\tilde{\alpha}(M)t\right)^{1/3}\right)\frac{M^2}{M^3 + 3\tilde{\alpha}(M)t}\frac{\tilde{\alpha}(M)}{M^2}\Big|_{M\to 0}, \tag{3.6}$$

which gives our final result

$$\boxed{\dot{n}_{\rm PBH} = \rho_{\rm DM}\frac{\psi_i\left(M_U\right)}{3t_U}} \tag{3.7}$$

with t_U the age of the universe, and $M_U = 3\tilde{\alpha}(0)t_U \simeq 5.1 \times 10^{14}$ g. This is one of the main results of our study.

Let us now derive an upper limit to the rate in Eq. (3.7) for a few representative mass functions. Consider the following three instances of well-motivated mass functions:

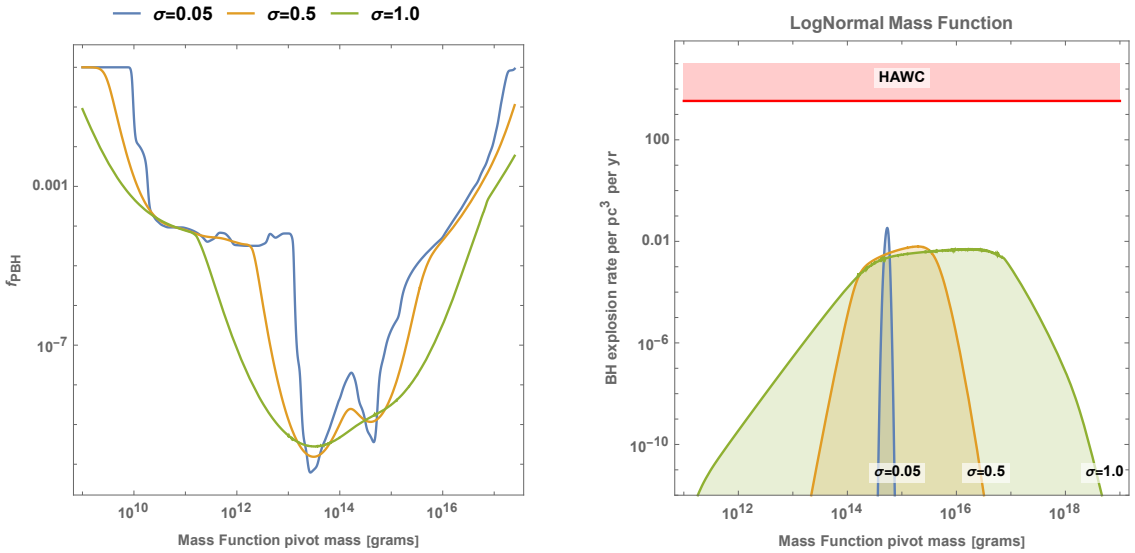

Figure 3. Left: The constraints on $f_{\rm PBH}$ as a function of the pivot mass M_* for the lognormal mass function of Eq. (3.8), for $\sigma = 0.05,\ 0.5$ and 1.0; Right: the maximal PBH explosion rate per unit volume, as a unction of the pivot mass M_*, for the same choices of σ as in the left panel.

1. Log-normal:

$$\psi(M, M_*, \sigma) = \frac{\exp\left(-\frac{\log(M/M_*)^2}{2\sigma^2}\right)}{\sqrt{2\pi}\sigma M}. \tag{3.8}$$

Fig. 3, left, shows the constraints, on the plane defined by the pivot mass M_* and $f_{\rm PBH}$, resulting from three different choices of $\sigma = 0.05,\ 0.5$ and 1.0, from Eq. (3.2). The right panel, again as a function of the pivot mass M_*, shows the explosion rate today, Eq. (3.7), for the maximal possible $f_{\rm PBH}$ at that pivot mass, again for $\sigma = 0.05,\ 0.5$ and 1.0.

The peak, for sufficiently narrow σ so that the variation in the constraints $f_{\rm PBH}(M_*, \sigma)$ is negligible, corresponds to $M_* = M_U$ so that the positive-definite argument of the exponential is 0; we find that

$$\dot{n}_{\rm PBH} \simeq \frac{1.2 \times 10^{-3}\ {\rm pc}^{-3}{\rm yr}^{-1}}{\sigma}, \tag{3.9}$$

implying that the current constraints from HAWC, at the level of 3400 pc^{-3} yr^{-1} [18], for this particular mass function constrain $\sigma \gtrsim 3.5 \times 10^{-7}$. For smaller values of σ the HAWC constraints *can* be violated while not violating the constraints on $f_{\rm PBH}$ at that given M_* (in other words, for sufficiently small σ the HAWC constraints are *the strongest* constraints on $f_{\rm PBH}$).

2. Power-law: here, the mass function is defined as

$$\psi(M, M_*, \gamma) = \frac{\gamma}{M}\left(\frac{M}{M_*}\right)^\gamma \ \text{for } M < M_*,\ 0 \text{ otherwise} \quad (\gamma > 0) \tag{3.10}$$

$$\psi(M, M_*, \gamma) = -\frac{\gamma}{M}\left(\frac{M}{M_*}\right)^\gamma \ \text{for } M > M_*,\ 0 \text{ otherwise} \quad (\gamma < 0). \tag{3.11}$$

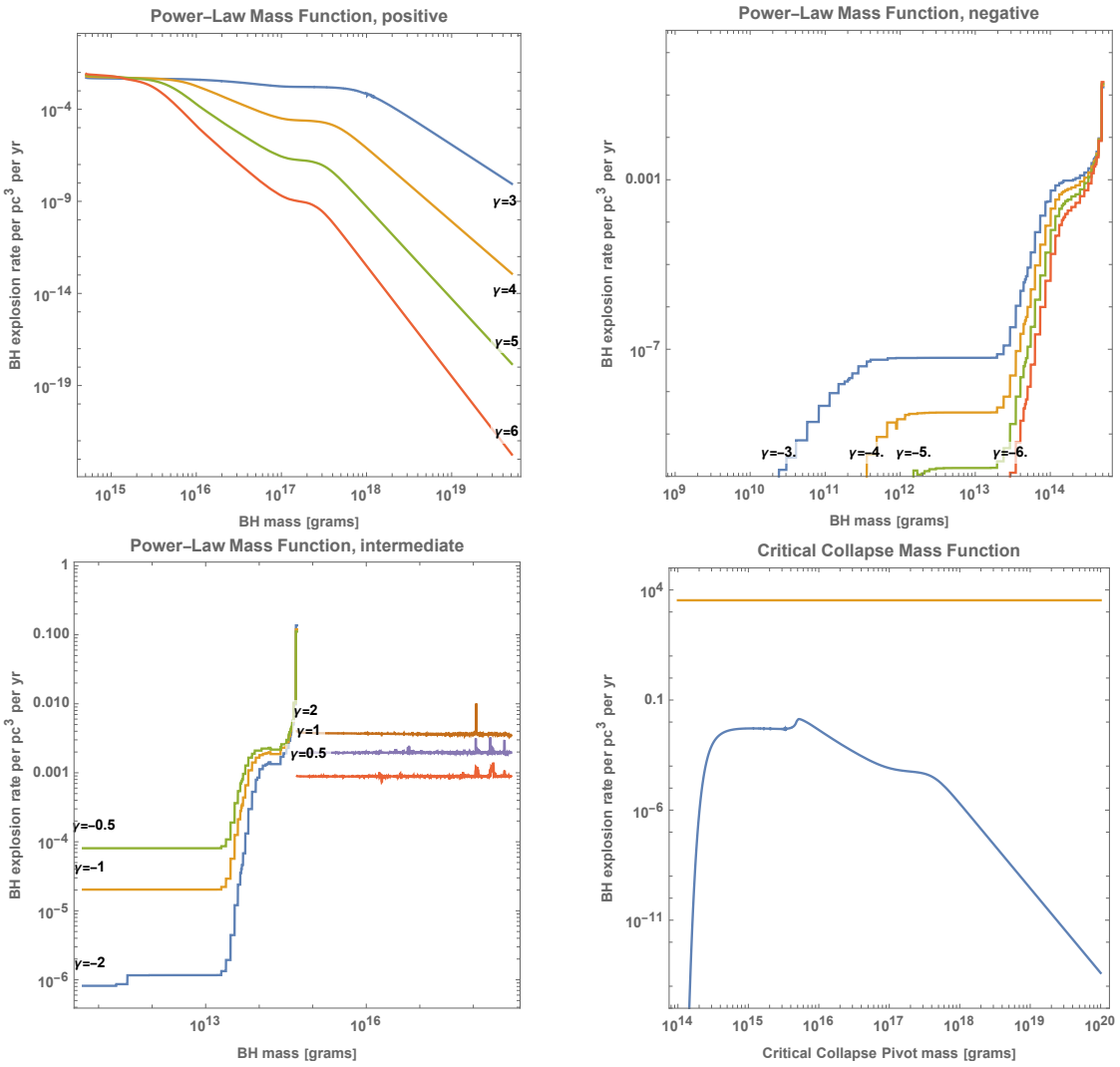

Figure 4. The PBH evaporation rate per unit volume, $\dot{n}_{\rm PBH}$, for the power-law mass function of Eq. (3.10-3.10), for large $|\gamma| \geq 3$ (top panels) and for intermediate $|\gamma| \leq 2$ (bottom, left); bottom, right: same but for the critical collapse mass function of Eq. (3.12).

In this case, evidently, the maximal explosion rate is achieved at $M_* = M_U$, and it corresponds to $\dot{n}_{\rm PBH} \sim 0.1$ pc^{-3}yr^{-1} for $\gamma < 0$ and to $\dot{n}_{\rm PBH} \sim 0.01$ pc^{-3}yr^{-1} for $\gamma > 0$, both rates linearly increasing with $|\gamma|$. We show the maximal PBH explosion rate $\dot{n}_{\rm PBH}$ as a function of M_* for positive (left) and negative (right) $|\gamma| \geq 3$ in the top panel of Fig. 4, for different values of γ. The bottom, left panel of the same figure shows again the explosion rate, for values of gamma in the intermediate $|\gamma| < 2$ range. In no case do we find a rate $\dot{n}_{\rm PBH}$ anywhere close to the current HAWC constraints.

3. Critical Collapse:

$$\psi(M, M_c) \propto M^{2.85} \exp\{-(M/M_c)^{2.85}\}. \tag{3.12}$$

In this case, we find that after taking into account the constraints on $f_{\rm PBH}$, the absolute maximum rate corresponds to a pivot mass $M_c \simeq 5.7 \times 10^{15}$ grams, and is approximately $\dot{n}_{\rm PBH} \sim 1.3 \times 10^{-2}$ pc^{-3}yr^{-1} (see Fig. 4, bottom right).

We note that there exist scenarios where PBH can be injected at very late times, where $\dot{n}_{\rm PBH}$ then depends on the injection rate and mass function at injection, but rather on late-times physics. This class of scenarios were recently reviewed and investigated in detail in Ref. [35, 36] to where we refer the interested Reader.

4 Sensitivity estimates and search strategies

We now proceed to compute updated estimates of the sensitivity of current and future gamma-ray detectors to exploding, light PBHs. To this end, we collected and digitized effective areas and angular resolution, as a function of energy, for the following detectors: BATSE [37], GBM [38], LAT [39], Veritas [40], HAWC [41], LHAASO [42] and CTA [43]; we also digitized the isotropic extragalactic background as measured by the LAT [44], with an extrapolation at very high energy of

$$\phi_B(E) = 1.4 \times 10^{-6} (E/\text{GeV})^{-2.1} \text{ cm}^{-2}\text{GeV}^{-1}\text{sec}^{-1}\text{sr}^{-1}. \tag{4.1}$$

We assume an optimal observing circumstance where the Galactic diffuse background is negligible compared to the extragalactic background (equivalently, we assume that the evaporating PBH is at high-enough Galactic latitude so that the Galactic diffuse emission is relatively negligible); for very high-energy gamma-ray telescopes we also add a background due to misidentified cosmic-ray events, with an appropriate instrument-specific rejection rate [40–43].

Given a PBH evaporating at a distance d, we adopt the following procedure to define a *detection*: we ask that a given telescope of effective area $A_{\rm eff}(E)$ and angular resolution corresponding to a solid angle $\Delta\Omega(E)$ can detect[2], in a statistically significant manner, a signal over background. As described in sec. 2 above, PBHs emit both primary and secondary photons (the latter from the decay into photons of other species produced upon evaporation) at a differential rate that depends on the black hole mass, and thus on time, $d^2N_\gamma(M_{\rm BH}(t))/(dt\ dE)$ sec^{-1} GeV^{-1}; assuming, as we do here, that the hole is spinless, the emission is isotropic, the flux of photons at the detector is

$$\phi_\gamma(E) = \frac{d^2N}{dt\ dE}(M_{\rm BH}(t))\frac{1}{4\pi d^2}. \tag{4.2}$$

The number of *signal* photons detected over an observation time $T_{\rm obs} = t_f - t_i$ is

$$N_S = \int dE \int_{t_i}^{t_f} dt \frac{d^2N}{dt\ dE}(M_{\rm BH}(t))\frac{A_{\rm eff}(E)}{4\pi d^2}. \tag{4.3}$$

Note that the relation between the time-to-expiration τ (i.e. time to complete evaporation, i.e. time till $T_{\rm BH} \to \infty$) and $M_{\rm BH}$ is, at low-enough BH masses, [4]:

$$\frac{\tau}{407 \text{ sec}} \simeq \left(\frac{M_{\rm BH}}{10^{10} \text{ gm}}\right)^3. \tag{4.4}$$

We need to specify the limits of integration in Eq. (4.3): while for the energy integral those are automatically taken care of by the $A_{\rm eff}(E)$, which goes to zero at very large and very small energies, for the time integral we have:

$$t_i = \theta\left(\tau - T_{\rm obs}\right); \quad t_f = \tau, \tag{4.5}$$

[2]The signal to noise is always maximized for the smallest possible angular region, which we assume to correspond to the instrumental angular resolution at a given energy.

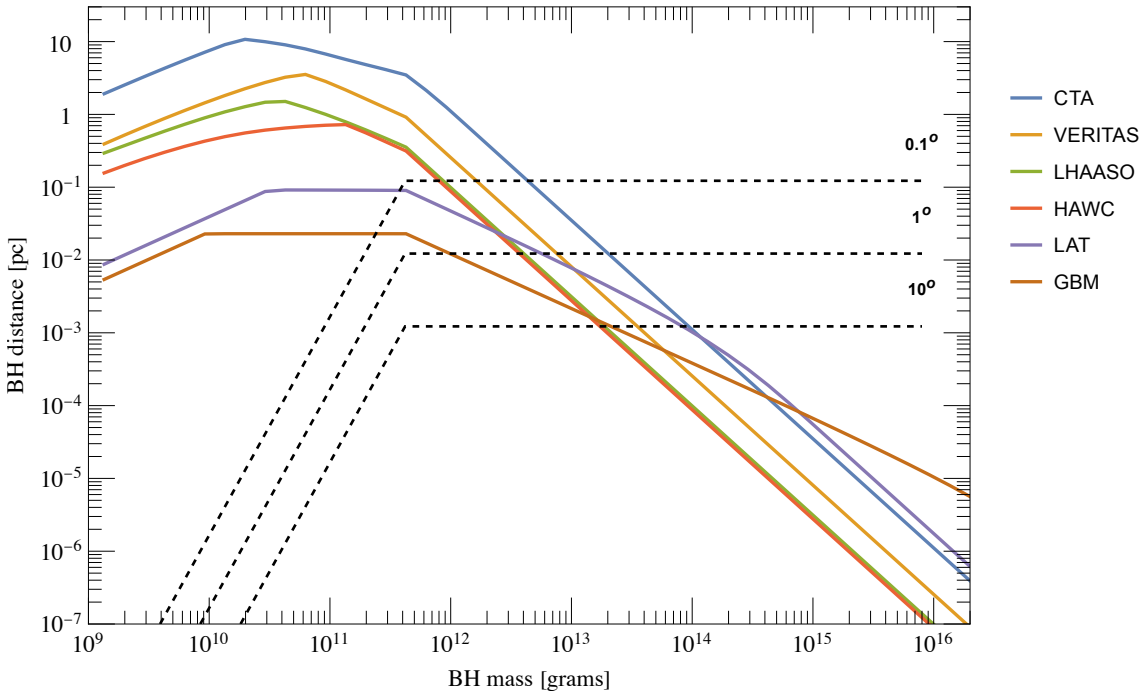

Figure 5. Maximum visible distance curves with respect to black hole mass for a number of modern gamma-ray detectors. The black dashed lines indicate the distance, at a given mass, at which the proper motion during an observation up to one year long may exceed 0.1, 1 and 10 degrees.

with θ the Heaviside step function. The number of *background* photons corresponding to the observation, meanwhile, is

$$N_B = \mathrm{Min}\,(T_{\rm obs}, \tau) \times \int dE\ \phi_B(E) A_{\rm eff}(E) \Delta\Omega(E). \tag{4.6}$$

Note that we neglect (i) the dead-time fraction of detectors, and (ii) the dependence of the effective area and angular resolution on the angular direction where the event occurs.

We ask for two conditions for a detection of a signal over background:

1. $N_S > 10$, i.e. to detect at least 10 signal photons;
2. $N_S/\sqrt{N_B} > 5$, i.e. that the approximate significance of the signal to background be larger than 5 sigma.

Adopting the formalism outlined above, we obtain the detector sensitivities shown in Fig. 5, in the plane defined by the black hole initial mass (or time to evaporation, related to the former by Eq. (4.4)) versus distance. Anything *below* the curves shown should be detectable by the corresponding facility. We also show, with dashed lines, the contours corresponding to the maximal proper motion in the sky during the relevant observation time, $\mathrm{Min}\,(T_{\rm obs}, \tau)$, assuming $T_{\rm obs} = 1$ yr. Above the dashed lines, proper motion is *below* the angular size shown on the plot. Notice that the angular proper motion depends on the angle ψ between the direction of motion of the PBH and the line of sigh direction; what we show corresponds to $\psi = 90°$, but for a generic ψ, the resulting angular proper motion is suppressed by a factor $\sin\psi$.

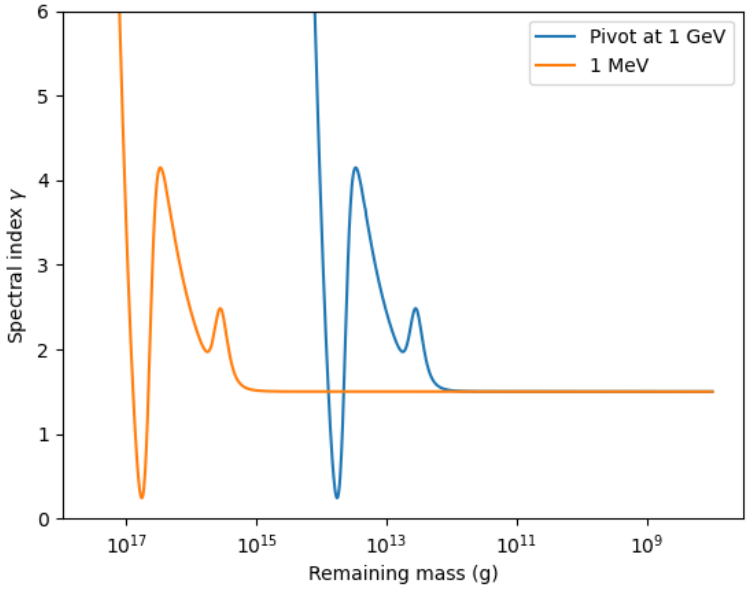

Figure 6. Spectral powerlaw index γ at 1 GeV and 1 MeV as a function of the evaporating BH mass.

Our findings illustrate that at present the best detector to discover evaporating black holes with a time-to-expiration τ shorter than a few years (equivalently, masses below, roughly 10^{12} grams) are Cherenkov telescope arrays; rather surprisingly, we find that the VERITAS array outperforms both HAWC and the future LHAASO telescopes, as a result of the effective area of VERITAS exceeding that of the other detectors in the critical range between a few 100 GeV and 10 TeV; for more massive and longer-lived PBHs, with masses between, approximately, 10^{13} and 10^{15} grams, the best currently-operating telescope is the LAT; for even more massive PBHs, the best telescopes are the smaller but lower-energy detectors GBM and BATSE (not shown, but similar to the GBM). The future CTA facility will outperform current observatories up to very large masses/low temperatures.

The facilities hierarchy we find depends primarily on a combination of the effective area of the telescopes, their angular resolution and background rejection capability, and on their energy range: the lighter the PBH, the higher the temperature etc, thus our results are not entirely unexpected. The specific shape of the sensitivity curves is also not unexpected, and it reflects, at short lifetimes/low masses (left), the time needed to accumulate a significant number of photons, while on the right there is mix of declining effective areas at lower energies, and a larger accumulated number of background photons. The most promising evaporating PBH for detection are in the few 10^{10} grams range (thus, objects that evaporate on time scales of the order of a few minutes), and located, at most, at a distance of a few parsecs, or $\sim 10^{19}$ m, or $\sim 10^{8}$ AU.

4.1 Spectral energy index

In addition to a universal lightcurve, barring non-standard additional degrees of freedom, PBH also feature a fully calculable and universal spectral evolution. In order to produce a quantity that is directly comparable to data, we compute with the `BlackHawk` code the slope of the *total differential photon* spectrum $\phi(E) = dN_\gamma/dE$ from an evaporating black hole of

a given mass, i.e. the spectral index $\gamma(E_0)$ at energy E_0,

$$\gamma(E_0) = \lim_{E\to E_0} \frac{E}{\phi(E)} \frac{d\phi(E)}{dE}. \tag{4.7}$$

We show in Fig. 6 the values of γ when the pivot energy is fixed at $E_0 = 1$ GeV (blue line) and at $E_0 = 1$ MeV (orange line), as a function of the black hole mass. Notice that at sufficiently large mass, γ grows very quickly due to the exponential decay in the emission spectrum. Importantly, the asymptotic spectral index, at sufficiently small PBH mass, is universal at $\gamma(M_{\rm PBH} \to 0) \to 1.5$, which will inform the observational campaign presented below.

4.2 The effect of proper motion

Proper motion describes changes in the angular position of objects in the sky as they are observed from Earth, and is an important observational quantity for long-term, relatively dim, nearby sources. Many observatories in the gamma-ray domain lack capability to associate long-term sources over wide angular variations: For example, the *Fermi*-LAT detection algorithm for transient sources considers sources with an error ellipse no greater than 15 degrees over the course of a decade of information (though observation windows for individual sources vary) [45].

We assume a PBH's average motion to be similar to the average Galactic dispersion $v \sim 220$km s^{-1} [46]; the relevant time-scales correspond, as above, to $min(\tau, T_{\rm obs})$. Here, τ is the remaining PBH lifetime and $T_{\rm obs}$ is the maximum telescope observation window (e.g. 10 years, with the *Fermi*-LAT transient catalog). Then, for a PBH distance d, traveling at an angle ψ with the line of sight,

$$\theta = \frac{180^\circ}{\pi} v \times \frac{min(\tau, T_{\rm obs})}{d} \times \sin\psi \tag{4.8}$$

At 0.01 parsecs, and for $\psi = 90^\circ$, this corresponds to, roughly, 1 degree per year. This jumps beyond 10 degrees per year at 0.001 parsecs. Association of gamma-ray sources over large periods of time is generally subject to choice of algorithm and variance in the gamma-ray background [47]. We consider the conservative bound which excludes any sources with proper motion exceeding order $\geq$10 degrees per year, that would be hard to conclusively associate to the same source. We also verified that the dimming/brightening effect for $\psi \sim 0,\ 180^\circ$ is consistently negligible.

4.3 Indirect detection of dark degrees of freedom

We seek to evaluate the detectability of the existence of a dark sector appearing at an mass/energy scale M_D corresponding, via Eq. (2.14), to a time-to-evaporation τ_D, and carrying a relative increase in degrees of freedom $\Delta\alpha/\alpha$. Motivated by our results shown in Fig. 5, we assume that a PBH "explosion" event occurred at a putative distance of 10^{-4} pc, and, for definiteness, that the event was detected by the Fermi LAT. On the plane defined by $(\tau_D, \Delta\alpha/\alpha)$, we compute the quantity $\tilde{\chi} \equiv \min(N_S^{\rm DS}/10,\ N_S^{\rm DS}/(5\sqrt{N_B}))$, where $N_S^{\rm DS}$ is the number of collected signal photons and N_B is the number of background photons (we described how these two quantities are evaluated in sec. 4 above). The quantity $\tilde{\chi}$ is, in practice, a proxy of whether a dark sector on the $(\tau_D, \Delta\alpha/\alpha)$ plane can be discerned from the standard model of PBH evaporation (i.e. absent additional, dark degrees of freedom).

If $\Delta\alpha/\alpha$ is not very large, the effect on the lightcurve may be too small to detect, unless the change happens during the observation window. On the other hand, if the dark sector

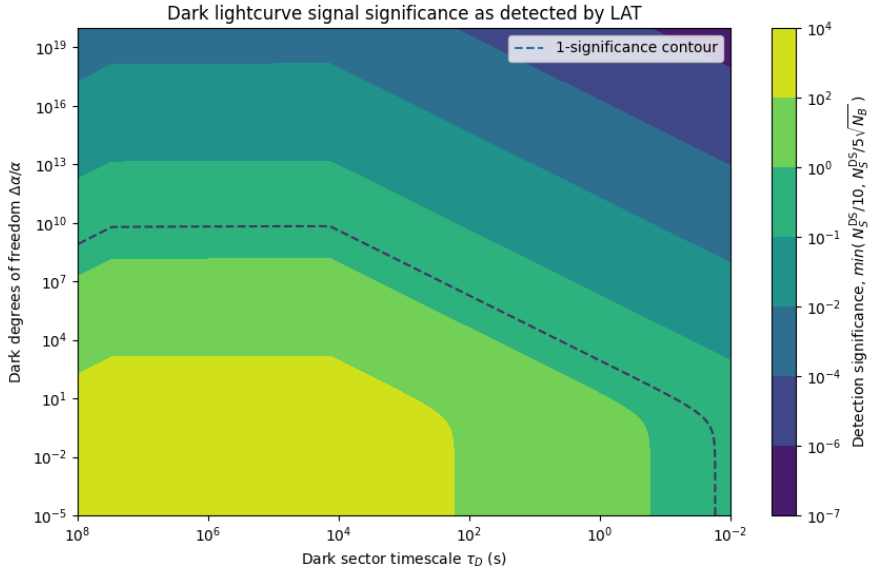

Figure 7. The effect of variations in $\Delta\alpha/\alpha$ and τ_D on the expected signal significance $\tilde{\chi} \equiv min(N_S^{\rm DS}/10, N_S^{\rm DS}/5\sqrt{N_B})$, for the Fermi-LAT detector, for a PBH at a distance of 10^{-4}pc. The decline at small values of τ_D is due to the LAT's decline in $A_{\rm eff}$ at $E \gg TeV$. We show the contour (dashed black) corresponding to the threshold at which we could detect the dark sector.

sets in too *late*, i.e. at very large energies, there is both too little time to accumulate enough isgnal events, and the photons might be too energetic to be detectable by the observatory at hand (here, the Fermi LAT). This explains the general shape of the "significance" contours, shown in Fig. 7. We note that, as shown in Fig. 1, if the dark sector sets in *outside* the time frame when evaporation is detected, then the signal appears identical to the standard case (up to a normalization difference). Of course, spectral information, correlating information on temperature as a function of time, could be used to disentangle the existence of a dark sector, at least in principle.

5 Searches for black hole explosions with Fermi LAT and GBM data

The projections derived above paint a relatively consistent picture for the possible domains in which a PBH could be detected by modern gamma-ray detectors. In confronting publicly available data sets, we consider two general scenarios: the detection of the very last, runaway phase of the BH "explosion", and the steady evaporation phase that precedes it. While the former is generally associated with a phenomenology similar (albeit different in significant ways, as mentioned in the Introduction) to that of a gamma-ray burst (GRB), the latter would manifest itself as a transient source with *increasing* luminosity (barring the effect of proper motion, that could dim the object as it moves away from the observer which, as mentioned above, is however negligible for the distances under consideration), and with a universal lightcurve and spectrum (again, barring the existence of significant dark-sector degrees of freedom, see sec. 4.3 above).

5.1 Long-term gamma-ray sources

In pursuit of long-term sources possibly associated with evaporating PBHs, we employ the LAT Transient Catalog [45]. This source catalog uses data collected from August 4th, 2008 to August 15, 2018 – over a decade of data. We foucs our analysis on "unnassociated" sources, labelled as such for weak correlation with any other known sources at other wavelengths [48]. At the time of retrieval, our query yielded lightcurves for 35 such unassociated sources.

We fit the lightcurve of these sources with a simple model consisting of two parameters: the distance d and the remaining PBH lifetime at initial detection, τ. We utilize a simple parameterization derived from the approximate differential photon yield integrated over the remaining lifetime, here τ, of an evaporating black hole. Calling $k_B T_\tau \approx 7.8$ TeV $(\tau/\text{sec})^{-1/3}$ the temperature corresponding to the remaining lifetime τ, Ref. [49, 50] finds, on the basis of HERWIG-based Monte Carlo simulations of the photon yield,

$$\frac{dN_\gamma}{dE_\gamma} \approx 9 \times 10^{35} \left(\frac{1\text{ GeV}}{k_B T_\tau}\right)^{3/2} \left(\frac{1\text{ GeV}}{E_\gamma}\right)^{3/2} \text{GeV}^{-1} \quad (E_\gamma < k_B T_\tau) \tag{5.1}$$

$$\frac{dN_\gamma}{dE_\gamma} \approx 9 \times 10^{35} \left(\frac{1\text{ GeV}}{E_\gamma}\right)^{3} \text{GeV}^{-1} \quad (E_\gamma \geq k_B T_\tau). \tag{5.2}$$

Considering the integrated flux above 0.1 GeV, we find that the integrated flux from a source at a distance d as a function of time from detection t (and indicating with τ again the remaining PBH lifetime at initial detection) reads, approximately,

$$F_\gamma(t, E_\gamma > 0.1\text{ GeV}) \simeq 2.7 \times 10^{-8} \left(\frac{\text{pc}}{d}\right)^2 \left(\frac{\tau - t}{\text{sec}}\right)^{-0.533} \text{cm}^{-2}\text{sec}^{-1}. \tag{5.3}$$

Note that this is also consistent with Eq. (2.3), when integrated over the same energy range. In what follows, we use Eq. (5.3) to fit for the distance and age of long-term evaporating PBHs.

Since the source continues to emit radiation, we use the observation window t_{obs} as a lower-bound on $\tau > t_{\text{obs}}$. This value is indicated in Fig. 5.1 as ΔMJD. We leave the remaining bounds for d and τ open. We assume that each error of each datapoint is Gaussian, and apply a non-linear least squares regression to each lightcurve for the lightcurve model of Eq. (5.3). The fitting process leaves wide errors for the model, owing to the small dataset size. We do not fit sources with a single datapoint, for which we independently calculate the standard error of the model with the 50% confidence intervals as shown. The fitted parameters for each source are given in Tab. 5.1, and the individual sources are shown in Fig. 5.1. We can very clearly see the resulting effect of the errors when we plot, in Fig. 9 our results on the same plane as Fig. 5.

We find that the sources, as expected, fall on the mass versus distance plane *below* the sensitivity predicted for the LAT, and they cluster into two groups: a first group, with masses around 10^{12} grams and distances of around a milliparsec, which exhibit a relatively fast-increasing lightcurve; and a second group, at masses between 10^{14} and 10^{15} grams and distances of $10^{-5} - 10^{-4}$ pc, with a slowly increasing lightcurve. The first set of sources are expcted to have proper motion in the few degrees range, on average. We note that this is *not consistent* with the fact that the LAT Transient Catalog [45] does not flag these sources as being associated with any proper motion. The second group of sources should have ever larger motion in the sky, several tens of degrees, again inconsistent with the LAT Transient

Catalog. We also note that the sources in the first, low-mass group should be detectable with operating high-energy gamma-ray Cherenkov telescopes, but such detections are lacking. All sources, finally, should have been detectable by GBM and/or BATSE, but again they were not. We thus conclude that *circumstantial evidence is strongly against the association of these long-term transient sources with evaporating, nearby PBHs.*

An additional, albeit inconclusive, test of whether the sources under consideration can be associated with evaporating PBH is to inspect the gamma-ray spectrum. As a proxy thereof, we compare, in Fig. 10, the spectral index γ at a gamma-ray energy of $E_0 = 1$ GeV, with the expected spectral index for evaporating PBHs shown in Fig. 6, as a function of the PBH lifetime left at initial detection τ. This quantity provides weak constraints due to the wide errors in the lifetime estimation. However, we note that the spectral indexes are generically *softer* than what expected for the light-mass cluster sources (i.e. γ is larger than predicted), while for the higher-mass cluster (corresponding in Fig. 10 to larger remaining lifetimes at detection, i.e. the left of the plot), the spectrum is inconsistent with the predicted exponential suppression, at least for the central values for τ.

Finally, we note that some sources with a high monotonic increase might indicate the sources could "explode" in the near future, with a handful broaching timescales in the next century, yielding the possibility that maximal flux will improve signal significance for other telescopes. This would benefit multi-spectral investigation of long-term PBH candidates, provided the detection and tracking of transient sources in other wavelengths is feasible. In the next section, we explore whether sources with even shorter variability time-scales could be tentatively associated with evaporating PBHs.

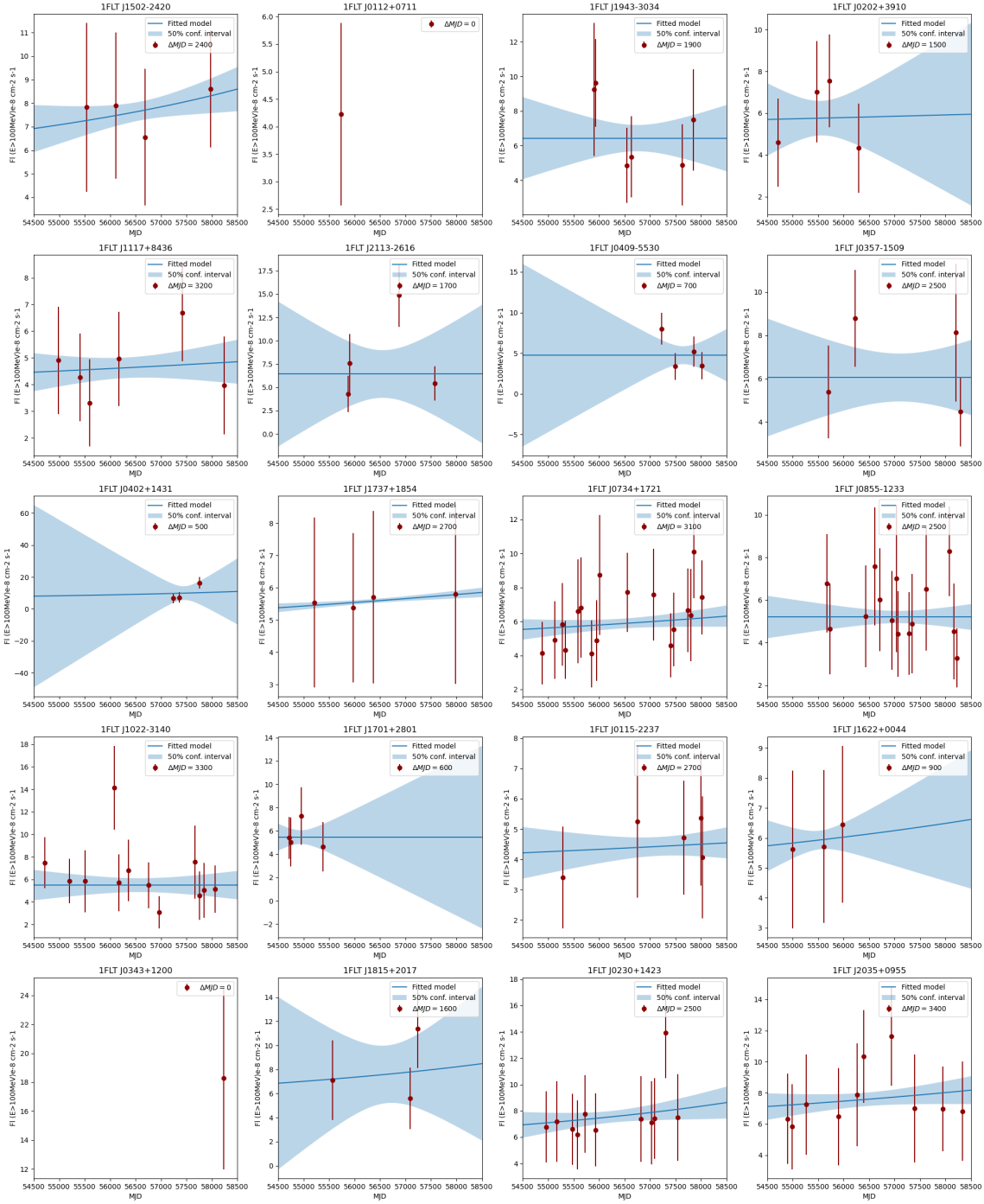
1FLT J1502-2420
Fitted model
50% conf. interval
ΔMJD = 2400
1FLT J0112+0711
ΔMJD = 0
1FLT J1943-3034
Fitted model
50% conf. interval
ΔMJD = 1900
1FLT J0202+3910
Fitted model
50% conf. interval
ΔMJD = 1500
1FLT J1117+8436
Fitted model
50% conf. interval
ΔMJD = 3200
1FLT J2113-2616
Fitted model
50% conf. interval
ΔMJD = 1700
1FLT J0409-5530
Fitted model
50% conf. interval
ΔMJD = 700
1FLT J0357-1509
Fitted model
50% conf. interval
ΔMJD = 2500
1FLT J0402+1431
Fitted model
50% conf. interval
ΔMJD = 500
1FLT J1737+1854
Fitted model
50% conf. interval
ΔMJD = 2700
1FLT J0734+1721
Fitted model
50% conf. interval
ΔMJD = 3100
1FLT J0855-1233
Fitted model
50% conf. interval
ΔMJD = 2500
1FLT J1022-3140
Fitted model
50% conf. interval
ΔMJD = 3300
1FLT J1701+2801
Fitted model
50% conf. interval
ΔMJD = 600
1FLT J0115-2237
Fitted model
50% conf. interval
ΔMJD = 2700
1FLT J1622+0044
Fitted model
50% conf. interval
ΔMJD = 900
1FLT J0343+1200
ΔMJD = 0
1FLT J1815+2017
Fitted model
50% conf. interval
ΔMJD = 1600
1FLT J0230+1423
Fitted model
50% conf. interval
ΔMJD = 2500
1FLT J2035+0955
Fitted model
50% conf. interval
ΔMJD = 3400
MJD
Fl (E>100MeV/e-8 cm-2 s-1

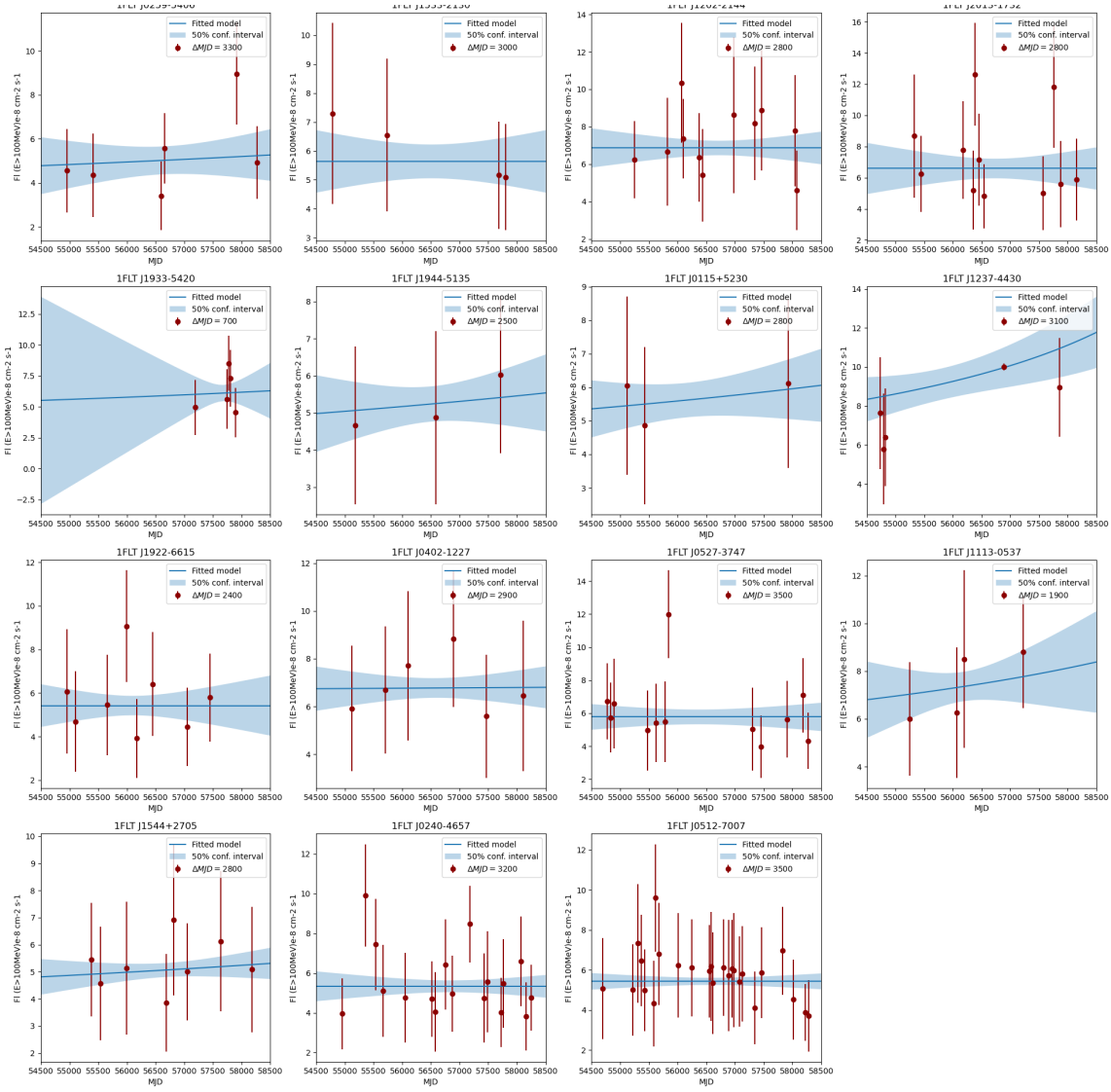

Figure 8. Parameterized powerlaw model (blue) with 50% confidence interval (blue shaded) for unassociated gamma-ray transients detected by the *Fermi*-LAT (red errorbars). Duration of the signal is shown for reference in Modified Julian Days, $T_{\rm obs} = \Delta MJD$.

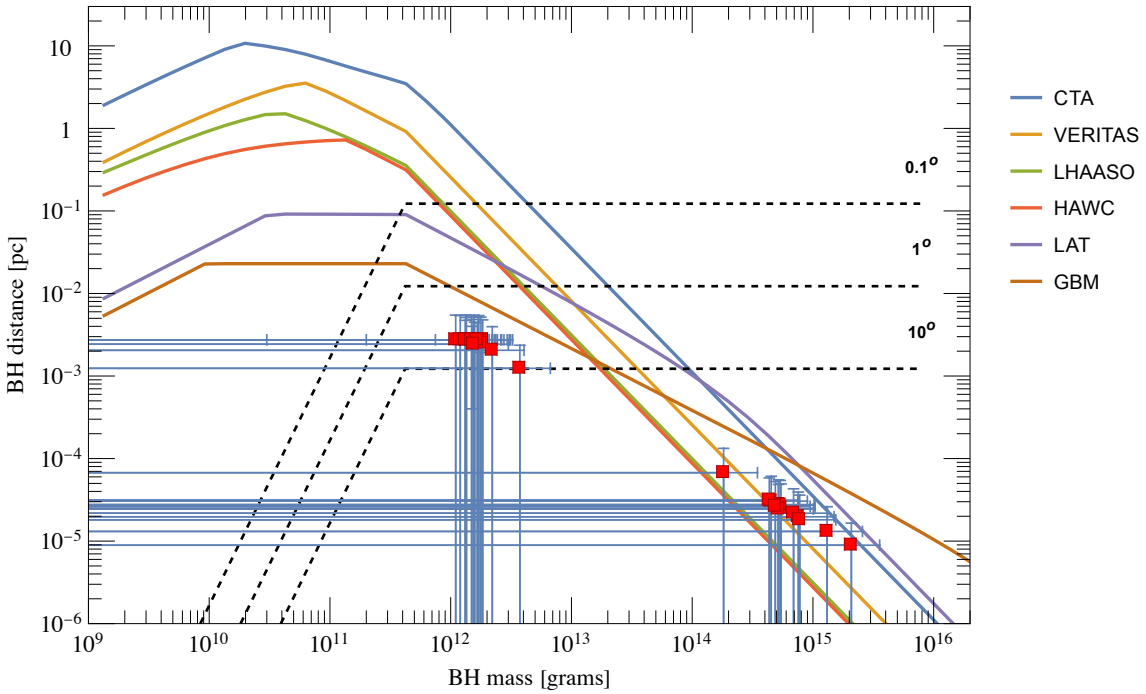

Figure 9. Transient fit results superimposed on the projected sensitivity limits described in previous sections.

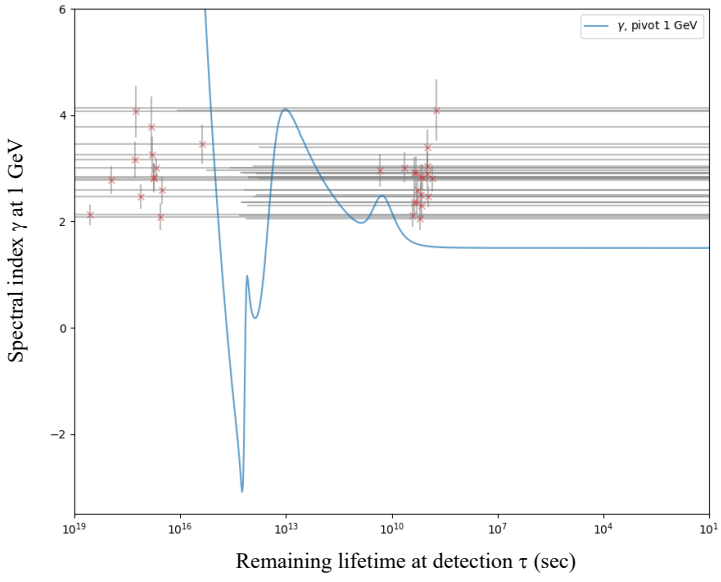

Figure 10. Lifetime and spectral index γ as fitted for the transient sources compared to the theoretical expectations for the same.

Source name	RA (deg)	DEC (deg)	τ (s)	τ u.l. (s)	τ l.l. (s)	d mpc)	d u.l. (pc)	d l.l. (pc)	γ	γ err.
1FLT J0115+5230	18.86	52.52	1.61E+09	1.25E+10	2.08E+08	2.74E-03	7.61E-03	9.83E-04	2.06	0.23
1FLT J0115-2237	18.96	-22.63	2.55E+09	4.05E+10	1.60E+08	2.74E-03	1.09E-02	6.86E-04	2.12	0.22
1FLT J0202+3910	30.60	39.17	4.41E+09	9.57E+11	2.03E+07	2.05E-03	3.02E-02	1.39E-04	3.01	0.29
1FLT J0230+1423	37.64	14.39	9.84E+08	2.53E+13	3.83E+04	2.74E-03	4.39E-01	1.71E-05	3.39	0.35
1FLT J0240-4657	40.16	-46.95	5.67E+16	3.22E+21	1.00E+12	2.77E-05	6.59E-03	1.16E-07	2.84	0.26
1FLT J0259-5406	44.84	-54.10	2.03E+09	2.55E+12	1.61E+06	2.74E-03	9.71E-02	7.71E-05	2.92	0.30
1FLT J0357-1509	59.40	-15.16	6.56E+16	8.76E+19	4.91E+13	2.50E-05	9.13E-04	6.84E-07	3.78	0.56
1FLT J0402-1227	60.51	-12.46	2.13E+10	2.22E+12	2.05E+08	1.24E-03	1.26E-02	1.22E-04	2.97	0.31
1FLT J0402+1431	60.66	14.52	5.39E+08	1.26E+16	2.30E+01	2.74E-03	1.32E+01	5.65E-07	4.10	0.59
1FLT J0409-5530	62.29	-55.50	2.44E+15	3.06E+18	1.95E+12	6.74E-05	2.38E-03	1.90E-06	3.46	0.36
1FLT J0512-7007	78.05	-70.13	9.21E+17	1.86E+22	4.55E+13	1.31E-05	1.86E-03	9.21E-08	2.77	0.27
1FLT J0527-3747	81.80	-37.79	1.77E+17	1.35E+22	2.32E+12	1.97E-05	5.43E-03	7.13E-08	4.07	0.49
1FLT J0734+1721	113.70	17.36	1.54E+09	6.17E+13	3.82E+04	2.74E-03	5.48E-01	1.36E-05	2.49	0.23
1FLT J0855-1233	133.75	-12.56	6.23E+16	3.48E+20	1.12E+13	2.73E-05	2.04E-03	3.66E-07	3.25	0.35
1FLT J1022-3140	155.74	-31.67	3.73E+16	1.93E+23	7.24E+09	3.05E-05	6.92E-02	1.34E-08	2.09	0.26
1FLT J1113-0537	168.36	-5.63	9.96E+08	5.51E+10	1.80E+07	2.74E-03	2.03E-02	3.68E-04	3.04	0.28
1FLT J1117+8436	169.28	84.62	2.31E+09	1.76E+11	3.02E+07	2.74E-03	2.39E-02	3.13E-04	2.92	0.29
1FLT J1202-2144	180.73	-21.74	5.63E+16	4.02E+20	7.87E+12	2.44E-05	2.07E-03	2.89E-07	2.81	0.27
1FLT J1237-4430	189.48	-44.51	7.03E+08	8.91E+11	5.55E+05	2.74E-03	9.74E-02	7.68E-05	2.81	0.25
1FLT J1502-2420	225.73	-24.34	9.38E+08	1.26E+10	6.97E+07	2.74E-03	1.00E-02	7.46E-04	2.46	0.19
1FLT J1533-2130	233.45	-21.50	3.67E+18	1.64E+20	8.21E+16	8.92E-06	5.96E-05	1.33E-06	2.12	0.19
1FLT J1544+2705	236.04	27.10	1.96E+09	1.20E+11	3.21E+07	2.74E-03	2.14E-02	3.50E-04	2.37	0.22
1FLT J1622+0044	245.71	0.74	1.42E+09	4.89E+09	4.13E+08	2.74E-03	5.07E-03	1.47E-03	2.30	0.25
1FLT J1701+2801	255.42	28.02	3.36E+16	1.54E+18	7.30E+14	3.14E-05	2.13E-04	4.63E-06	2.59	0.25
1FLT J1737+1854	264.27	18.90	2.27E+09	3.43E+09	1.50E+09	2.50E-03	3.07E-03	2.03E-03	2.36	0.27
1FLT J1815+2017	273.95	20.29	9.53E+08	1.34E+13	6.79E+04	2.74E-03	3.24E-01	2.31E-05	2.90	0.27
1FLT J1922-6615	290.61	-66.25	1.34E+17	1.66E+20	1.09E+14	2.18E-05	7.67E-04	6.22E-07	2.47	0.24
1FLT J1933-5420	293.42	-54.34	1.34E+09	4.59E+11	3.91E+06	2.74E-03	5.06E-02	1.48E-04	2.83	0.25
1FLT J1943-3034	295.91	-30.57	4.74E+16	2.47E+20	9.09E+12	2.64E-05	1.91E-03	3.66E-07	3.01	0.17
1FLT J1944-5135	296.12	-51.60	1.85E+09	1.23E+10	2.79E+08	2.74E-03	7.04E-03	1.06E-03	2.59	0.20
1FLT J2013-1732	303.50	-17.55	1.91E+17	3.45E+23	1.05E+11	1.81E-05	2.43E-02	1.34E-08	3.16	0.34
1FLT J2035+0955	308.90	9.92	1.48E+09	1.16E+13	1.89E+05	2.43E-03	2.15E-01	2.75E-05	2.84	0.24
1FLT J2113-2616	318.37	-26.27	4.58E+27	7.67E+34	2.73E+20	3.24E-08	1.33E-04	7.93E-12	4.14	0.58

Table 1. Gamma-ray LAT transients, also shown in Fig. 5.1, with relevant statistics and fitted parameters.

5.2 Short-duration GRB-like sources

In searching for events potentially associated with the last phase of PBH evaporation, we use the Fermi GBM Burst Catalog, which lists high-energy sources detected in 14 years of operation [51–54]. We impose the following criteria on the lightcurve evolution and on the spectrum:

1. In the GBM energy range, the expectation for the ratio $t_{90}/t_{50} \simeq 2.4$, which is a proxy for the lightcurve evolution with time for exploding PBHs (here t_{50} and t_{90} indicate the time taken to accumulate 50% (90%) of the burst fluence starting at the 25% (respectively, 5%) fluence level)

2. For a pivot energy below the GeV, the spectral index is expected to follow $d\phi_\gamma/dE \sim E^{-\gamma_{\rm PBH}}$ with $\gamma_{\rm PBH} \simeq 1.5$, the late-time asymptote shwon in Fig. 6.

For both quantities, we utilize the values of t_{90}, t_{50}, and γ listed in the GBM event catalogue. We include all sources that are 2σ within the predicted values of t_{90}/t_{50} and $\gamma_{\rm PBH}$. The resulting list of candidate sources amounts to the 388 shown in Fig. 11, left, with yellow x's, on the plane defined by the spectral index versus the t_{90}/t_{50} ratio (the vertical and horizontal lines indicate the PBH expected values).

Fig. 11, right, shows the sky distribution of both the GRB events (again indicated as yellow x's) and the unassociated transient sources discussed above. We note a fairly homogeneous sky distribution for both classes of events. In particular, we find that the ratio of sources in the northern to southern hemisphere is 1.04, whereas the ratio of sources in the western to eastern hemispheres is 0.879 – indicating a slightly larger abundance in the eastern hemisphere of the sky. The theoretical expectation for PBH events, stemming from the relative position of the Earth within the Milky Way dark matter halo in Galactic coordinates, and assuming no PBH clustering [55] is of order 0.02%, assuming a standard Navarro-Frenk-White [56] dark matter density profile (no asymmetry is expected in the east vs west emispheres). We note that previous studies of very-short GRBs using the BATSE monitor discovered a similar overdensity in the eastern hemisphere, caused possibly by halo clumping [57]. Note also that isotropy is an indication of extragalactic gamma-ray sources, disfavoring, but not ruling out, a Galactic origin such as PBH explosions. Possible future directions in this area include pursuing solar neighborhood-localized bursts utilizing a network of GRB detectors, as suggested in [24].

5.3 Possible association of long-term transient and GRB sources with evaporating PBHs

Here, we search for events where a long-term, unassociated, transient source from the LAT catalogue discussed in sec. 5.1 could be associated with a gamma-ray burst, accounting for proper motion. We consider any event where the difference between the LAT and GRB localization for right ascension (RA) and declination (DEC), accounting for uncertainties in the angular determination $\Delta\theta$, and allowing for 1 degree of proper motion per year (corresponding, approximately, to sources within 0.01 pc, the typical maximal distance for detection by the LAT) scaled by time (the initial detection time for the transient source and $t_0^{\rm trans.}$ and the GRB burst time $t^{\rm grb}$).

$$\begin{aligned}\sqrt{\left(\mathrm{RA}^{\rm grb}-\mathrm{RA}^{\rm trans.}\right)^2+\left(\mathrm{DEC}^{\rm grb}-\mathrm{DEC}^{\rm trans.}\right)^2}-\left(\Delta\theta^{\rm grb}+\Delta\theta^{\rm trans.}\right)\\ \leq \frac{1\mathrm{deg}}{\mathrm{yr}}\times\left(t^{\rm grb}-t_0^{\rm trans.}\right)\end{aligned} \tag{5.4}$$

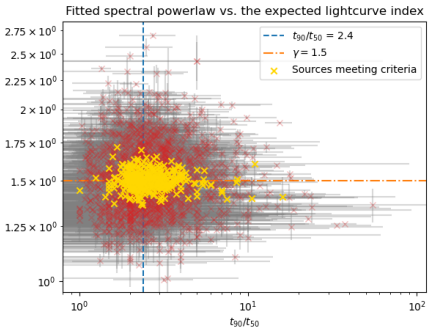

Figure 11. Candidate GRB events possibly compatible with PBH evaporation, on the $\gamma, t_{90}/t_{50}$ plane.

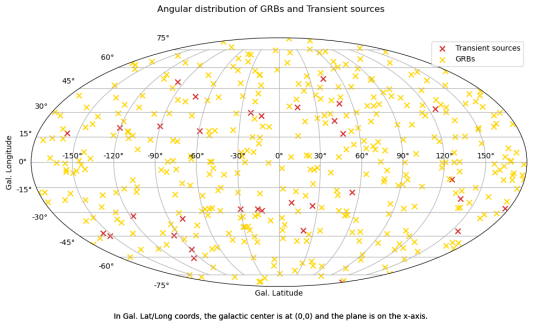

Figure 12. Angular distribution of PBH-candidate GRBs and Transient gamma-ray sources as catalogued in the GBM and Transient source catalogs.

Of the 35 transient sources, we find 14 which have at least one GRB detected within the above limit. In an ideal case, the GRB follows the last (most recent) observation of a transient source and appears brighter than its transient counterpart as it corresponds with the final, runaway PBH explosion. Fig. 13 shows the lightcurves of the possible associations, in conjunction with the tentatively associated GRB events. The relevant catalog information and data are listed in Table 5.3. For all the fitted transient sources, the corresponding GRBs lie well outside the confidence interval to be associated with the standard PBH lightcurve, albeit in some cases the association is not obviously ruled out.

We additionally inspected the lightcurves of all individual GRBs listed in Tab. 5.3. In most cases, the presence of an "afterglow" strongly rules out the association of the event with the last stage of an evaporating PBH: as shown conclusively in Ref. [58], no "photosphere", and therefore no afterglow can form around an evaporating PBH. Of all sources, the one GRB that, statistically, could be marginally compatible with the lightcurve of an evaporating PBH is GRB141213300, shown in Fig. 14. We show there the signal from the four GBM detectors, the NaI (colored n1, n2, n5) and BGO (grey b0) detectors, binned on 100ms and overlain with their average (black). This source typifies many of the ideal characteristics in a candidate PBH GRB, including sharp rising and falling edges. Additionally, the higher-energy BGO detector has a slightly higher countrate and leads the NaI detectors by $\sim$ 100ms. Intriguingly, GRB141213300 lies within the scaled ROI of 1FLT J1701+2801 (see Fig. 13).

6 Discussion, conclusions, and further directions

The potential of directly observing a PBH explosion carries far-reaching implications for our understanding of the universe, from cosmology, to quantum gravity, to particle physics. While the existence of PBHs as a candidate for dark matter has been theorized for decades, direct detection of an evaporating PBH would provide invaluable insights into yet-undiscovered high-energy particles and dark radiation.

In this study, we have reviewed photon emission from the late-stage evaporation of PBHs, including the effect of the existence of "dark" degrees of freedom on the expected lightcurve. We produced a compact expression for the rate of evaporation of PBH as a function of their time-evolved mass function, and obtained upper limits on the local rate of PBH evaporation for several different mass functions. We showed that it is possible, albeit not expected, to

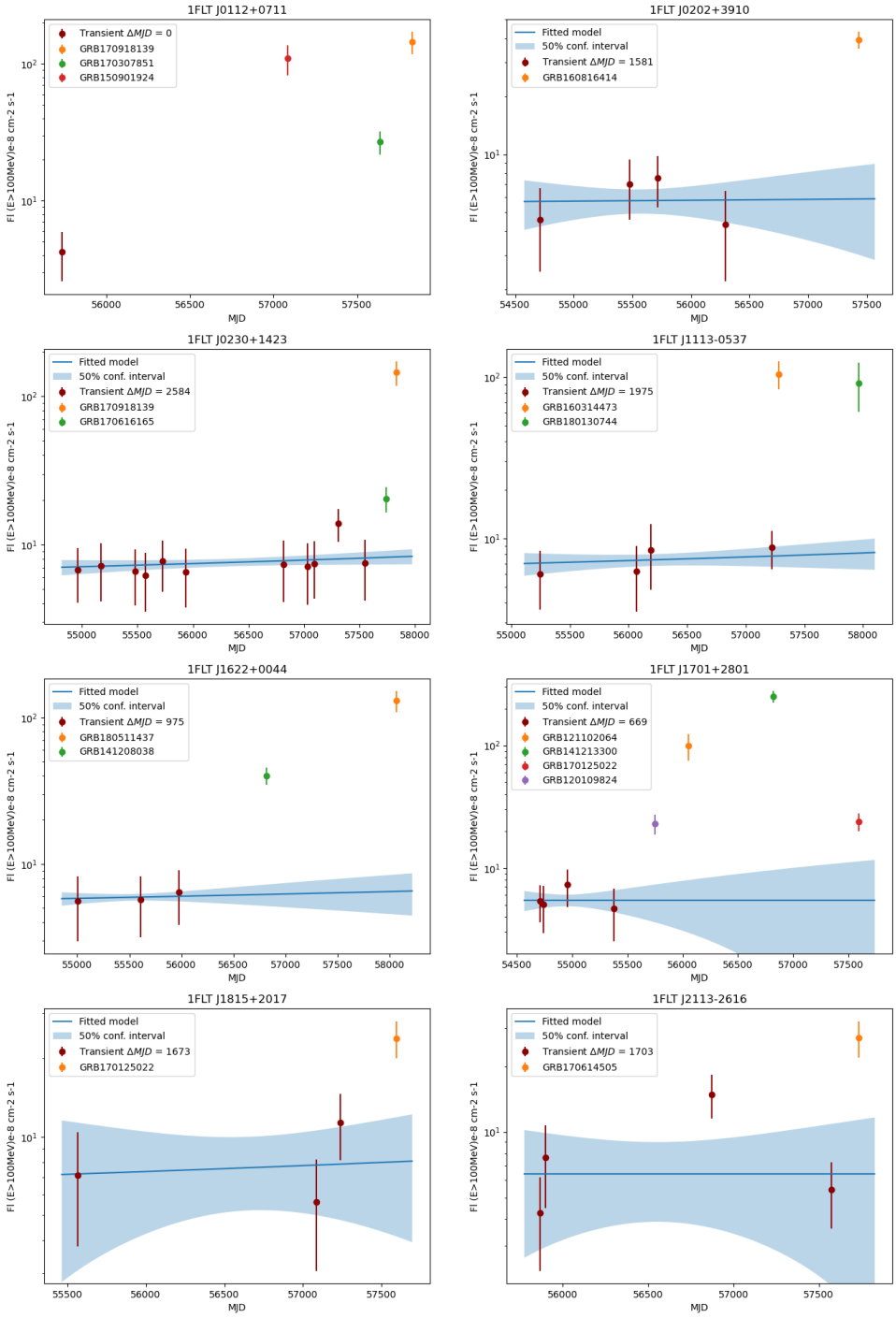

Figure 13. For each LAT transient source, we plot the flux of tentatively associated GRBs.

Source name	RA (deg)	DEC (deg)	Rad. Err. (deg)	Flux (erg/cm^2/s)	Flux err.	t_{90}/t_{50}	t_{90}/t_{50} err.
GRB170614505	310.99	-37.91	15.16	2.71e-07	5.19e-08	2.10	1.62
GRB160314473	161.99	2.83	19.99	1.04e-06	2.04e-07	8.67	15.87
GRB170918139	36.56	3.52	17.81	1.45e-06	2.67e-07	4.00	6.96
GRB180511437	257.78	9.07	10.16	1.30e-06	2.09e-07	2.58	1.78
GRB170307851	13.54	9.54	0.05	2.69e-07	5.10e-08	2.06	0.79
GRB141208038	239.16	10.97	9.49	4.01e-07	5.41e-08	1.93	0.57
GRB150901924	16.34	13.52	17.12	1.09e-06	2.73e-07	2.00	9.29
GRB121102064	258.47	14.09	12.15	9.90e-07	2.45e-07	1.60	1.52
GRB141213300	248.19	18.06	8.72	2.49e-06	2.72e-07	4.00	3.62
GRB170616165	49.51	19.67	12.12	2.04e-07	3.93e-08	2.27	0.74
GRB170125022	264.14	28.58	12.65	2.40e-07	3.93e-08	2.44	1.49
GRB120109824	251.33	30.80	11.33	2.29e-07	4.15e-08	2.25	0.72
GRB160816414	25.32	43.70	19.13	3.93e-07	3.94e-08	2.19	1.53
GRB180130744	136.83	52.69	68.08	9.20e-07	3.14e-07	2.00	7.58

Source name	MJD (days)	t_{90} (s)	t_{90} err.	γ	γ pos. err.	γ neg. err.
GRB170614505	5.77e+04	5.38	1.64	-1.45	0.12	0.12
GRB160314473	5.73e+04	1.66	0.73	-1.51	0.13	0.13
GRB170918139	5.78e+04	0.13	0.16	-1.45	0.08	0.08
GRB180511437	5.81e+04	1.98	0.97	-1.52	0.10	0.10
GRB170307851	5.76e+04	28.42	1.72	-1.57	0.10	0.10
GRB141208038	5.68e+04	14.34	1.45	-1.49	0.07	0.07
GRB150901924	5.71e+04	0.26	1.15	-1.40	0.17	0.17
GRB121102064	5.60e+04	2.05	1.38	-1.52	0.16	0.16
GRB141213300	5.68e+04	0.77	0.51	-1.54	0.05	0.05
GRB170616165	5.77e+04	56.32	6.08	-1.39	0.12	0.12
GRB170125022	5.76e+04	3.90	1.12	-1.45	0.10	0.10
GRB120109824	5.58e+04	38.66	3.11	-1.50	0.11	0.11
GRB160816414	5.74e+04	11.78	3.81	-1.54	0.06	0.06
GRB180130744	5.80e+04	0.26	0.92	-1.53	0.23	0.23

Table 2. Data and fitting parameters for the GRB sources in Fig. 13, with relevant statistics. Note that MJD is Modified Julian Days.

have evaporation rates as large as the current observational limits from the HAWC telescope; more plausible rates hover around a few per tens of parsec cubed per year.

We then built an updated estimate of detector sensitivities across detectors as small as the Gamma-ray burst monitor onboard the Fermi satellite, and as large as LHAASO. We computed the maximal distance where an exploding PBH with a given lifetime to expiration could be detected by a given telescope. We showed that the peak sensitivity is reached for lifetimes on the order of 100 to 10^7 sec, corresponding to masses in the ton to several hundred tons. We showed how larger detectors such as VERITAS and HAWC, and future detectors such as CTA and LHAASO are best suited to detect lighter PBHs (i.e. PBHs at later evaporation stages), while detectors such as LAT and GBM are best suited to detect heavier, and closer-by PBHs.

We studied the features of gamma-ray signals from PBH evaporation such as the spectral power-law index, that could help disentangle astrophysical, standard sources from PBHs; we evaluated the importance of source proper motion, and estimated the features of dark sectors (such as the energy-scale and the number of degrees of freedom) that could be detectable given the discovery of an exploding PBH.

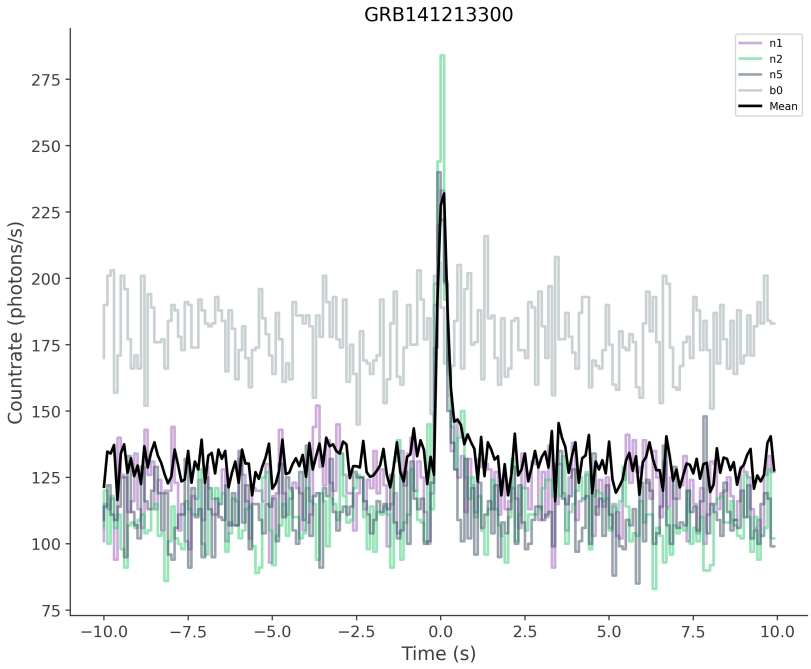

Figure 14. The lightcurve of GRB141213300, for the four GBM detectors, and the corresponding mean (black); the event lies within the scaled ROI of 1FLT J1701+2801.

Sec. 5 was devoted to actual searches for exploding PBH in gamma-ray data from the Fermi satellite. We first focused on long-term variable, unassociated "transient" sources from the LAT Transient Catalog. We individually fit the lightcurves of the transient sources, and computed best-fit values for both the distance and the remaining PBH lifetime at initial detection; the sources cluster at extrapolated distances of (i) a few milliparsec and lifetimes of 10^8-10^9 sec, corresponding to masses around 10^{12} grams, or at (ii) distances around a few tens of microparsecs, and lifetimes on the order of 10^{16}-10^{19} sec, corresponding to masses in the 10^{14} to 10^{15} grams range; the two clusters correspond to "fast rising" vs slow rising" transients. We noticed how our fits, however, have very large uncertainty in both distance and time to evaporation/mass. Additionally, the sources, if indeed associated with local evaporating PBHs should generally have significant proper motion, which they don't, and should have been observed by other observatories besides the LAT, which hey haven't. We also studied the spectral properties of such long-term transients, and found that, even though, once again, the uncertainties are very significant, the spectra are not *per se* incompatible with what expected from PBH evaporation, especially for the fast rising trnasient sources.

We then explored short-duration GRB-like sources, and selected, amongts the Fermi GBM Burst Catalog, sources with the correct lighcurve proxy, t_{90}/t_{50}, and spectral power-law index. We singled out close to 400 candidate sources, distributed roughly homogeneously in the sky. Further association of such searches with PBH evaporation events requires closer spectral inspection, and the possible association with long-term transient. Taking into account proper motion, we extracted a set of 8 possible associated long- and short-term sources; of these, one appears to have a lightcurve roughly compatible with the absence of an afterglow (within statistical uncertainties). However, while our analysis did not produce any conclusive evidence of such association, it offers a framework for future studies and observations.

Overall, the potential for direct detection of a PBH explosion holds immense promise for advancing our understanding of the universe. As observational and theoretical analysis capabilities continue to improve, further investigation and refinements of the constraints presented in this study will undoubtedly lead to new insights in the physics of evaporating black holes.

Acknowledgments

This work was supported in part by the U.S. Department of Energy grant number desc0010107 (SP).

References

[1] Particle Data Group collaboration, *Review of Particle Physics*, *PTEP* **2022** (2022) 083C01.

[2] A. Addazi et al., *Quantum gravity phenomenology at the dawn of the multi-messenger era—A review*, *Prog. Part. Nucl. Phys.* **125** (2022) 103948 [2111.05659].

[3] J. Auffinger, *Primordial black hole constraints with Hawking radiation – a review*, 2206.02672.

[4] B. Carr, K. Kohri, Y. Sendouda and J. Yokoyama, *Constraints on primordial black holes*, *Rept. Prog. Phys.* **84** (2021) 116902 [2002.12778].

[5] S. Bird et al., *Snowmass2021 Cosmic Frontier White Paper: Primordial black hole dark matter*, *Phys. Dark Univ.* **41** (2023) 101231 [2203.08967].

[6] T.N. Ukwatta, D.R. Stump, J.T. Linnemann, J.H. MacGibbon, S.S. Marinelli, T. Yapici et al., *Primordial Black Holes: Observational Characteristics of The Final Evaporation*, *Astropart. Phys.* **80** (2016) 90 [1510.04372].

[7] M.J. Baker and A. Thamm, *Probing the particle spectrum of nature with evaporating black holes*, *SciPost Phys.* **12** (2022) 150 [2105.10506].

[8] M.J. Baker and A. Thamm, *Black hole evaporation beyond the Standard Model of particle physics*, *JHEP* **01** (2023) 063 [2210.02805].

[9] B.V. Lehmann, C. Johnson, S. Profumo and T. Schwemberger, *Direct detection of primordial black hole relics as dark matter*, *JCAP* **10** (2019) 046 [1906.06348].

[10] S.W. Hawking, *Black hole explosions*, *Nature* **248** (1974) 30.

[11] B.J. Carr and S.W. Hawking, *Black holes in the early Universe*, *Monthly Notices of the Royal Astronomical Society* **168** (1974) 399.

[12] T.N. Ukwatta, J.H. MacGibbon, W.C. Parke, K.S. Dhuga, S. Rhodes, A. Eskandarian et al., *Sensitivity of the FERMI Detectors to Gamma-Ray Bursts from Evaporating Primordial Black Holes (PBHs)*, in *12th Marcel Grossmann Meeting on General Relativity*, pp. 1588–1590, 3, 2010, DOI [1003.4515].

[13] H.E.S.S. collaboration, *Limits on Primordial Black Hole evaporation with the H.E.S.S. array of Cherenkov telescopes*, in *33rd International Cosmic Ray Conference*, p. 0930, 7, 2013 [1307.4898].

[14] HESS collaboration, *Limits on primordial black hole evaporation from H.E.S.S. observations*, *PoS* **ICRC2021** (2021) 518.

[15] A.A. Abdo et al., *Milagro Limits and HAWC Sensitivity for the Rate-Density of Evaporating Primordial Black Holes*, *Astropart. Phys.* **64** (2015) 4 [1407.1686].

[16] Fermi-LAT collaboration, *Search for Gamma-Ray Emission from Local Primordial Black Holes with the Fermi Large Area Telescope*, *Astrophys. J.* **857** (2018) 49 [1802.00100].

[17] VERITAS collaboration, *Search for Primordial Black Hole Evaporation with VERITAS*, *PoS* **ICRC2017** (2018) 691 [1709.00307].

[18] HAWC collaboration, *Constraining the Local Burst Rate Density of Primordial Black Holes with HAWC*, *JCAP* **04** (2020) 026 [1911.04356].

[19] D.B. Cline and W. Hong, *Very short gamma-ray bursts and primordial black hole evaporation*, *Astropart. Phys.* **5** (1996) 175.

[20] D.B. Cline, *The Search for GRB from primordial black hole evaporation*, *Astrophys. Space Sci.* **231** (1995) 393.

[21] D.B. Cline, D.A. Sanders and W. Hong, *Further evidence for gamma-ray bursts consistent with primordial black hole evaporation*, *Astrophys. J.* **486** (1997) 169.

[22] D.B. Cline, *Primordial black holes and short gamma-ray bursts*, *Phys. Rept.* **307** (1998) 173.

[23] D.B. Cline, S. Otwinowski, B. Czerny and A. Janiuk, *Do Very Short Gamma Ray Bursts originate from Primordial Black Holes? Review*, *Int. J. Astron. Astrophys.* **1** (2011) 164 [1105.5363].

[24] T.N. Ukwatta et al., *Investigation of Primordial Black Hole Bursts using Interplanetary Network Gamma-ray Bursts*, *Astrophys. J.* **826** (2016) 98 [1512.01264].

[25] B.J. Carr, *Some cosmological consequences of primordial black-hole evaporations*, *Astrophys. J.* **206** (1976) 8.

[26] M. Korwar and S. Profumo, *Updated constraints on primordial black hole evaporation*, *JCAP* **05** (2023) 054 [2302.04408].

[27] F. Halzen, B. Keszthelyi and E. Zas, *Neutrinos from primordial black holes*, *Phys. Rev. D* **52** (1995) 3239 [hep-ph/9502268].

[28] A. Ejlli, D. Ejlli, A.M. Cruise, G. Pisano and H. Grote, *Upper limits on the amplitude of ultra-high-frequency gravitational waves from graviton to photon conversion*, *Eur. Phys. J. C* **79** (2019) 1032 [1908.00232].

[29] A. Ireland, S. Profumo and J. Scharnhorst, *Primordial gravitational waves from black hole evaporation in standard and nonstandard cosmologies*, *Phys. Rev. D* **107** (2023) 104021 [2302.10188].

[30] A. Arbey and J. Auffinger, *BlackHawk: a public code for calculating the hawking evaporation spectra of any black hole distribution*, *The European Physical Journal C* **79** (2019) .

[31] J.H. MacGibbon and B.R. Webber, *Quark and gluon jet emission from primordial black holes: The instantaneous spectra*, *Phys. Rev. D* **41** (1990) 3052.

[32] H. Davoudiasl, P.B. Denton and D.A. McGady, *Ultralight fermionic dark matter*, *Phys. Rev. D* **103** (2021) 055014 [2008.06505].

[33] B. Carr, M. Raidal, T. Tenkanen, V. Vaskonen and H. Veermäe, *Primordial black hole constraints for extended mass functions*, *Phys. Rev. D* **96** (2017) 023514 [1705.05567].

[34] F. Halzen, E. Zas, J.H. MacGibbon and T.C. Weekes, *Gamma-rays and energetic particles from primordial black holes*, *Nature* **353** (1991) 807.

[35] Z.S.C. Picker and A. Kusenko, *Explaining the GeV excess with exploding black holes*, 2305.13434.

[36] Z.S.C. Picker and A. Kusenko, *Constraints on late-forming exploding black holes*, 2305.13429.

[37] D. Band et al., *BATSE observations of gamma-ray burst spectra. 1. Spectral diversity.*, *Astrophys. J.* **413** (1993) 281.

[38] C. Meegan et al., *The Fermi Gamma-Ray Burst Monitor*, *Astrophys. J.* **702** (2009) 791 [0908.0450].

[39] Fermi-LAT collaboration, *The Large Area Telescope on the Fermi Gamma-ray Space Telescope Mission*, *Astrophys. J.* **697** (2009) 1071 [0902.1089].

[40] T.C. Weekes et al., *VERITAS: The Very energetic radiation imaging telescope array system*, *Astropart. Phys.* **17** (2002) 221 [astro-ph/0108478].

[41] HAWC collaboration, *On the sensitivity of the HAWC observatory to gamma-ray bursts*, *Astropart. Phys.* **35** (2012) 641 [1108.6034].

[42] LHAASO collaboration, *The Large High Altitude Air Shower Observatory (LHAASO) Science Book (2021 Edition)*, *Chin. Phys. C* **46** (2022) 035001 [1905.02773].

[43] CTA Consortium collaboration, *Introducing the CTA concept*, *Astropart. Phys.* **43** (2013) 3.

[44] Fermi-LAT collaboration, *The Spectrum of the Isotropic Diffuse Gamma-Ray Emission Derived From First-Year Fermi Large Area Telescope Data*, *Phys. Rev. Lett.* **104** (2010) 101101 [1002.3603].

[45] F.-L.C. L. Baldini et. al., *Catalog of long-term transient sources in the first 10 yr of fermi-lat data*, *The Astrophysical Journal Supplement Series* **256** (2021) 13.

[46] J. Binney and S. Tremaine, *Galactic Dynamics*, Princeton series in astrophysics, Princeton University Press (1987).

[47] F. Kunzweiler, B. Biltzinger, J. Greiner and J.M. Burgess, *Automatic detection of long-duration transients in gbm data*, *Astronomy & Astrophysics* **665** (2022) A112.

[48] Fermi-LAT collaboration, *A Statistical Approach to Recognizing Source Classes for Unassociated Sources in the First Fermi-LAT Catalog*, *Astrophys. J.* **753** (2012) 83 [1108.1202].

[49] E. Bugaev, P. Klimai and V. Petkov, *Photon spectra from final stages of a primordial black hole evaporation in different theoretical models*, in *30th International Cosmic Ray Conference*, vol. 3, pp. 1123–1126, 6, 2007 [0706.3778].

[50] V.B. Petkov et al., *Searching for Very-High-Energy Gamma-Ray Bursts from Evaporating Primordial Black Holes*, *Astron. Lett.* **34** (2008) 509 [0808.3093].

[51] F.C. A. von Kienlin et. al., *The fourth fermi-gbm gamma-ray burst catalog: A decade of data*, *The Astrophysical Journal* **893** (2020) 46.

[52] F.C. David Gruber et. al, *The fermi gbm gamma-ray burst spectral catalog: Four years of data*, *The Astrophysical Journal Supplement Series* **211** (2014) 12.

[53] F.C. Andreas von Kienlin et. al., *The second fermi gbm gamma-ray burst catalog: The first four years*, *The Astrophysical Journal Supplement Series* **211** (2014) 13.

[54] F.C. P. Narayana Bhat et. al, *The third fermi gbm gamma-ray burst catalog: The first six years*, *The Astrophysical Journal Supplement Series* **223** (2016) 28.

[55] M. Gorton and A.M. Green, *Effect of clustering on primordial black hole microlensing constraints*, *JCAP* **08** (2022) 035 [2203.04209].

[56] J.F. Navarro, C.S. Frenk and S.D.M. White, *The Structure of cold dark matter halos*, *Astrophys. J.* **462** (1996) 563 [astro-ph/9508025].

[57] D. Cline, C. Matthey and S. Otwinowski, *Evidence for a galactic origin of very short gamma ray bursts and primordial black hole sources*, *Astroparticle Physics* **18** (2003) 531.

[58] J.H. MacGibbon, B.J. Carr and D.N. Page, *Do Evaporating Black Holes Form Photospheres?*, *Phys. Rev. D* **78** (2008) 064043 [0709.2380].